Calibration of the 1D shallow water equations: a comparison of Monte Carlo and gradient-based optimization methods

Asier Lacasta, Mario Morales-Hernández, Javier Burguete, Pilar Brufau and Pilar García-Navarro

ABSTRACT

The calibration of parameters in complex systems usually requires a large computational effort. Moreover, it becomes harder to perform the calibration when non-linear systems underlie the physical process, and the direction to follow in order to optimize an objective function changes depending on the situation. In the context of shallow water equations (SWE), the calibration of parameters, such as the roughness coefficient or the gauge curve for the outlet boundary condition, is often required. In this work, the SWE are used to simulate an open channel flow with lateral gates. Due to the uncertainty in the mathematical modeling that these lateral discharges may introduce into the simulation, the work is focused on the calibration of discharge coefficients. Thus, the calibration is performed by two different approaches. On the one hand, a classical Monte Carlo method is used. On the other hand, the development and application of an adjoint formulation to evaluate the gradient is presented. This is then used in a gradient-based optimizer and is compared with the stochastic approach. The advantages and disadvantages are illustrated and discussed through different test cases.

Key words | adjoint method, calibration, gradient method, Monte Carlo, shallow water equations

Asier Lacasta (corresponding author)
Mario Morales-Hernández
Pilar Brufau
Pilar García-Navarro
Fluid Mechanics,
LIFTEC, CSIC-Universidad Zaragoza,
Maria de Luna 3,
Zaragoza 50018,
Spain
E-mail: *alacasta@unizar.es*

Javier Burguete
Soil and Water, EEAD/CSIC,
P.O. Box 13034,
Zaragoza 50080,
Spain

INTRODUCTION

Calibration is related to the optimization process of finding the minimum of a functional usually defined as a relation between the objective quantity and that simulated. There are many fields where calibration is required. This process is more necessary when using black-box models or simplified deterministic models. In some ways, the model may acquire a predictive character when calibrated. The calibration can be understood as an optimization process, where the error between the model estimate and the data set is minimized.

In addition, there are many phenomena that can be modeled using partial differential equations (PDEs) that represent conservation laws. The application of mathematical models to describe physical processes is helpful when performing simulations of possible scenarios using computational facilities (Burguete *et al.* 2014). Despite the quality of these mathematical models for predictive purposes, some parameters underlie the simplifications in the model. Consequently, calibration is usually required to adjust the model to the physical reality (Lacasta *et al.* 2015b).

The application of the shallow water equations (SWE) for the simulation of open-channel flow has been widely used, in particular, for irrigation water delivery (Chanson 2004; Chaudhry 2007). The equations can also be extended to include regulation elements. The flow in those hydraulic structures does not follow the shallow water hypothesis. Their presence is usually modeled by means of steady state continuity and head loss equations that somehow represent what lies behind these phenomena (Morales-Hernández *et al.* 2013).

doi: 10.2166/hydro.2017.021

There are three broad optimizer families: gradient-based methods, derivative-free search algorithms, and evolutionary methods (Chaparro *et al.* 2008). This work deals with the first and second families. While the latter do not require gradient information to perform the calibration, the former must have information about the variation of the objective function with respect to the controlled variable. The advantage of these methods appears when the performance function is sufficiently smooth, and the first derivative, with respect to the controllable parameter, drives the optimization method to the optimal value. On the contrary, and when local minima exist, these methods can be inefficient and may also provide non-optimal solutions. These situations can be avoided using other global optimization methods not based on gradient information, such as stochastic methods. While they can probably more easily detect the optimal interval in the global solution space, they are expensive in terms of evaluations.

In this case, the use of Lagrange multipliers within variational principles leads to the definition of adjoint variables and the corresponding differential equations governing them. Their solutions can help to obtain the sensitivity of a pre-defined objective function. This family of methods has largely been developed over the last 30 years (Giles & Pierce 2000). However, and due to increasing computational capacity, adjoint methods have been applied in different forms in many fields: from airfoil shape optimal design (Castro *et al.* 2007; Bueno-Orovio *et al.* 2012) to estimating *Greeks* in the financial derivatives industry (Giles & Glasserman 2006). In the context of free surface flow hydraulics, the use of the adjoint method to obtain the adjoint system of equations intended for control was described in Sanders & Katopodes (2000), Piasecki & Sanders (2002), and Ding & Wang (2006). Interesting applications have also been recently described for data assimilation (Lai & Monnier 2009; Lacasta & García-Navarro 2016) and field data reconstruction (Lacasta *et al.* 2015a). Such works highlight the capacity of the adjoint method for providing an estimate of the gradient that can be used for control purposes. Regarding hydraulic model calibration, the widest application is the identification of roughness parameters. There are several works on this, such as Fread & Smith (1978) and Wasantha Lal (1995). In addition, in Pappenberger *et al.* (2005), an application of a Monte Carlo (MC)-based optimization procedure for roughness parameter identification can be found, while in Ding & Wang (2005), the adjoint equations of the one-dimensional (1D) SWE are used for the same purpose.

The non-linear SW flow equations must be solved numerically and this can be done by different numerical methods. Several techniques applied to such equations have been reported recently as promising, such as second-order MUSCL schemes (Hou *et al.* 2015) and higher order numerical schemes (Díaz *et al.* 2013; Navas-Montilla & Murillo 2015). Also, the emerged discontinuous Galerkin method has been used to compute them (Xing *et al.* 2010; Kesserwani & Liang 2015; Kesserwani *et al.* 2015). Despite the apparent good properties of these methods, the enormous computational need may be a drawback when dealing with practical applications. In addition, not only the accuracy, but also the quality in terms of conservation and well-balancing of the numerical solution is desirable when dealing with these equations (Noelle *et al.* 2006). The use of a first order upwind (FOU) scheme, such as that of Murillo & García-Navarro (2010), has been demonstrated to be a good option because of the acceptable trade-off between numerical quality and computational requirements. In the context of SWE, the use of first-order schemes is common, since in the majority of the flows concerning realistic applications, the source terms dominate over the convective terms, second-order diffusive terms are not included in the formulation and the difference between the numerical results from first- and second-order models becomes negligible (Petaccia & Savi 2002; Murillo *et al.* 2009). In this work, forward solver and adjoint solver are both based on a well-balanced and exhaustively tested FOU finite volume scheme.

The objective of this work is to compare two widely used approaches for the calibration of a computational model based on the SWE. On the one hand, a gradient descent (GD) method is used as an example of gradient-based optimization. On the other hand, the use of MC following the method of Burguete & Latorre (2015) is included as an example of *brute-force* calibration methodology. In this work, the calibration is aimed at the estimation of a discharge coefficient in order to model the outflow from a lateral hydraulic structure. In order to evaluate the performance of each technique, three cases different in nature are proposed. They are related to the calibration of (1) an approximately

reachable situation (the error in the optimal solution is not equal to zero), (2) an affordable target level at some point, and (3) an affordable target level located in a position separated by an internal boundary condition (a sluice gate). The structure of the paper is as follows: below, the mathematical model and the adjoint formulation are described. The next section includes the numerical scheme used to obtain a discrete solution for both problems and then the mathematical optimization problem is formulated, emphasizing the gradient-free optimization method used in this work as well as the gradient formulation based on the adjoint information. This is followed by a section in which the gradient-based optimizer and MC method are compared in three different cases, and finally, conclusions are drawn.

MATHEMATICAL MODEL

Shallow water equations

The 1D SWE or Saint-Venant equations derive from the cross-sectional-averaged Navier–Stokes equations of mass ($\mathbf{G_1}$) and momentum ($\mathbf{G_2}$) under the hypothesis of incompressible flow and mild bed slope. They form a 2×2 hyperbolic system of equations (Cunge *et al.* 1980; Chanson 2004; Chaudhry 2007). A one-dimensional flow in a unitary fixed-width channel can be expressed as follows:

$$\begin{aligned}\mathbf{G_1}&: \frac{\partial h}{\partial t}+\frac{\partial q}{\partial x}-q_l=0\\ \mathbf{G_2}&: \frac{\partial q}{\partial t}+\frac{\partial}{\partial x}\left(\frac{q^2}{h}+\frac{gh^2}{2}\right)-gh(S_0-S_f)=0\end{aligned} \tag{1}$$

where the conserved variables (h, q) are the water depth and unitary discharge, respectively defined in space $x \in [x_0, x_L]$ and time $t \in [0, T]$ and g the gravitational acceleration.

In addition, S_f is related to the friction slope, represented by the empirical Gauckler–Manning's law, and S_0 is related to the bed slope:

$$S_f=\frac{q|q|n^2}{h^2R_h^{4/3}},\quad S_0=-\frac{\partial z}{\partial x} \tag{2}$$

where n is the Gauckler–Manning's roughness coefficient, and the bed slope depends on bottom depth z. Additionally, the hydraulic radius $R_h = A/P$ is the ratio of the channel's cross-sectional area A to the wetted perimeter P. The lateral discharge is considered as a mass sink term that can be formulated as:

$$q_l = K_g G_0 \sqrt{h} \tag{3}$$

where h is the upstream water depth at the gate location and G_0 is the gate opening. Figure 1 illustrates a channel including a lateral gate as described. It is important to take into account that (3) deals with the formulation of a simplistic Bernoulli-based formulation of the flow assuming atmospheric pressure downstream of the gate. This implies that the discharge rate depends only on the water depth upstream of the gate. K_g can be used to account for some uncertainties related to losses due to different causes such as construction irregularities, and obstruction or bed changes from sediment deposition with slope changes. This quantity is bounded by $0 < K_g < \sqrt{2g}$ when realistic situations are simulated (Henderson 1996). The source

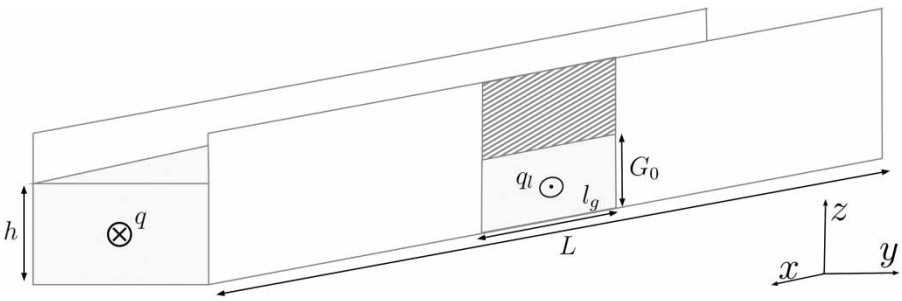

Figure 1 | Sketch of the channel.

term in (3) is defined at the location of the gate and it is assumed that it will vanish in the rest of the channel. It is important to note that some authors (Piasecki & Sanders 2002; Baume *et al.* 2005; Fovet *et al.* 2010) include the lateral flow influence in the momentum equation, whereas others, such as Malaterre *et al.* (1998), Ding & Wang (2006), and Xu *et al.* (2011), prefer to neglect that effect. In this work, the lateral offtake is considered a point mass contribution ($l_g \to 0$) without effect on the momentum equation.

Performance function

The aim of the optimization problem is to reach an objective which can be defined as the target water depth $h(x, t)_{\text{obj}}$. A functional that includes the target is defined as follows:

$$\mathbf{J} = \int_0^T \int_{x_0}^{x_L} \mathcal{E}(x, t; h, q) dx dt = \frac{1}{2} \int_0^T \int_{x_0}^{x_L} (h(x, t) - h(x, t)_{\text{obj}})^2 dx dt \quad (4)$$

where $(0, T)$ is the simulated time period and (x_0, x_L) are the coordinates of the reach under consideration. The error metric $\mathcal{E}$ may be defined by considering N_p measured water depths. A very typical function to measure the deviation between an estimation and a measurement is the mean square error (MSE) which may include saddles, but no local minimum; this may be convenient for some minimization methods.

Adjoint formulation

Depending on the kind of optimizer used to perform the minimization, information regarding sensitivities is required. In the gradient-based methods, the gradient is used as a sensitivity measurement that is able to conduct the optimizer to the minimum. The adjoint system can be obtained introducing a Lagrange multiplier field and assuming first-order optimality conditions (Cassel 2013). Then, an augmented functional is defined based on (4) as $\mathbf{J}^+ = \mathbf{J} + \mathbf{P}$, where $\mathbf{P}$ is obtained by multiplying the mass conservation equation ($\mathbf{G_1}$) by the adjoint variable (also known as Lagrange multiplier) $\sigma_1(x, t)$ and the momentum conservation equation ($\mathbf{G_2}$) by the adjoint variable $\sigma_2(x, t)$:

$$\mathbf{P} = \int_0^T \int_{x_0}^{x_L} [\sigma_1(\mathbf{G_1}) + \sigma_2(\mathbf{G_2})] dx dt \quad (5)$$

$\mathbf{P}$ can be integrated by parts leading to:

$$\mathbf{P} = \int_0^T \int_{x_0}^{x_L} \left[-h\frac{\partial \sigma_1}{\partial t} - q\frac{\partial \sigma_1}{\partial x} - q\frac{\partial \sigma_2}{\partial t} - \left(\frac{q^2}{h} + \frac{gh^2}{2}\right)\frac{\partial \sigma_2}{\partial x} - \sigma_1 q_l - \sigma_2 gh(S_o - S_f) \right] dx dt + \int_{x_0}^{x_L} [\sigma_1 h + \sigma_2 q]|_0^T dx + \int_0^T \left[\sigma_1 q + \sigma_2 \left(\frac{q^2}{h} + \frac{gh^2}{2}\right) \right] \Big|_{x_0}^{x_L} dt \quad (6)$$

Assuming first order optimality condition for $\mathbf{J}^+$

$$\delta \mathbf{J}^+ = \delta \mathbf{J} + \delta \mathbf{P} = 0 \quad (7)$$

These variations $\delta \mathbf{J}^+$ on (7) can be formulated taking increments with respect to h and q. Since in this case we need to adjust the discharge coefficient K_g, variations of (6) with respect to its dependent variable K_g are also included leading to:

$$\delta \mathbf{P} = \int_0^T \int_{x_0}^{x_L} \left[-\delta h\frac{\partial \sigma_1}{\partial t} - \delta q\frac{\partial \sigma_1}{\partial x} - \delta q\frac{\partial \sigma_2}{\partial t} - \left(2\frac{q}{h}\delta q - \frac{q^2}{h^2}\delta h + gh\delta h\right)\frac{\partial \sigma_2}{\partial x} - \sigma_2 g\delta h(S_o - S_f) + \sigma_2 gh\left(\frac{\partial S_f}{\partial q}\delta q + \frac{\partial S_f}{\partial h}\delta h\right) + \sigma_1\left(\frac{\partial q_l}{\partial h}\delta h + \frac{\partial q_l}{\partial K_g}\delta K_g\right) \right] dx dt + \int_{x_0}^{x_L} [\sigma_1 \delta h + \sigma_2 \delta q]|_0^T dx + \int_0^T \left[\sigma_1 \delta q + \sigma_2 \left(\frac{2q}{h}\delta q - \frac{q^2}{h^2}\delta h + gh\delta h\right) \right] \Big|_{x_0}^{x_L} dt \quad (8)$$

Increments are also taken in the objective function $\mathbf{J}$:

$$\delta \mathbf{J} = \int_0^T \int_{x_0}^{x_L} \left(\frac{\partial \mathcal{E}}{\partial h}\delta h + \frac{\partial \mathcal{E}}{\partial q}\delta q + \frac{\partial \mathcal{E}}{\partial K_g}\delta K_g\right) dx dt \quad (9)$$

Considering (7), whenever the following is satisfied:

$$\tilde{\mathbf{G}}_1: -\frac{\partial \sigma_1}{\partial t} + \left(\frac{q^2}{h^2} - gh\right)\frac{\partial \sigma_2}{\partial x} - g\sigma_2(S_0 - S_f) + g\sigma_2 h\frac{\partial S_f}{\partial h} + \sigma_1\frac{\partial q_l}{\partial h} + \frac{\partial \mathcal{E}}{\partial h} = 0 \quad \tilde{\mathbf{G}}_2: -\frac{\partial \sigma_2}{\partial t} - \frac{\partial \sigma_1}{\partial x} - 2\frac{q}{h}\frac{\partial \sigma_2}{\partial x} + \sigma_2 gh\frac{\partial S_f}{\partial q} + \frac{\partial \mathcal{E}}{\partial q} = 0 \quad (10)$$

$\delta \mathbf{J}$ can be rewritten as:

$$\delta \mathbf{J} = \overbrace{\int_{x_0}^{x_L} [\sigma_1 \delta h + \sigma_2 \delta q]|_0^T dx}^{(a)} + \overbrace{\int_0^T \left[\sigma_1 \delta q + \sigma_2 \left(\frac{2q}{h}\delta q - \left(\frac{q^2}{h^2} - gh\right)\delta h\right)\right]\Big|_{x_0}^{x_L} dt}^{(b)} + \underbrace{\int_0^T \int_{x_0}^{x_L} \sigma_1 \frac{\partial q_l}{\partial K_g}\delta K_g + \frac{\partial \mathcal{E}}{\partial K_g}\delta K_g dx dt}_{(c)} \tag{11}$$

Imposing initial conditions for $\delta h, \delta q$ and final conditions for σ_1, σ_2 in (11a):

$$\begin{aligned} &\sigma_1(x, T) = 0, \sigma_2(x, T) = 0, \qquad x_0 < x < x_L \\ &\delta h(x, 0) = 0, \delta q(x, 0) = 0, \qquad x_0 < x < x_L \end{aligned} \tag{12}$$

as well as boundary conditions for $\delta h, \delta q$ in (11b):

$$\begin{aligned} &\delta h(x_0, t) = 0, \delta q(x_0, t) = 0, \delta h(x_L, t) = 0, \delta q(x_L, t) \\ &\qquad = 0, \\ &0 < t < T \end{aligned} \tag{13}$$

the final expression of (11) leads to the evaluation of $\delta \mathbf{J}$ as (11c):

$$\delta \mathbf{J} = \int_0^T \int_{x_0}^{x_L} \sigma_1 \frac{\partial q_l}{\partial K_g}\delta K_g + \frac{\partial \mathcal{E}}{\partial K_g}\delta K_g dx dt \tag{14}$$

Equation (14) is then defined as the sensitivity of the error and will be very useful in the development of the gradient expression to be included in the optimization method. Due to the dependence on (14) with respect to σ_1, (10) must be solved numerically.

NUMERICAL SCHEME

There are two systems to be solved: the physical equations (1) and the adjoint equations (10). Both have the same aspect from the mathematical point of view since they are hyperbolic systems of equations and can be treated in a similar way. The first is system (1), comprising $(\mathbf{G_1}, \mathbf{G_2})$. This system can be written in a non-conservative form as:

$$\frac{\partial \mathbf{U}}{\partial t} + \mathbf{M}\frac{\partial \mathbf{U}}{\partial x} = \mathbf{S} \tag{15}$$

where

$$\begin{aligned} &\mathbf{U} = \begin{pmatrix} h \\ q \end{pmatrix}, \quad \mathbf{M} = \begin{pmatrix} 0 & 1 \\ c^2 - u^2 & 2u \end{pmatrix}, \\ &\mathbf{S} = \begin{pmatrix} q_l \\ gh(S_0 - S_f) \end{pmatrix} \end{aligned} \tag{16}$$

where $u = q/h$ is the velocity and $c = \sqrt{gh}$ the wave celerity. The second is the adjoint system (10) comprising $(\tilde{\mathbf{G}}_1, \tilde{\mathbf{G}}_2)$:

$$-\frac{\partial \mathbf{\Psi}}{\partial t} + \mathbf{\Gamma}\frac{\partial \mathbf{\Psi}}{\partial x} = \mathbf{R} \tag{17}$$

where

$$\begin{aligned} &\mathbf{\Psi} = \begin{pmatrix} \sigma_1 \\ \sigma_2 \end{pmatrix}, \quad \mathbf{\Gamma} = \begin{pmatrix} 0 & u^2 - c^2 \\ -1 & -2u \end{pmatrix}, \\ &\mathbf{R} = \begin{pmatrix} -\dfrac{\partial \mathcal{E}}{\partial h} + g\sigma_2\left[S_0 - S_f - h\dfrac{\partial S_f}{\partial h}\right] + \sigma_1 \dfrac{\partial q_l}{\partial h} \\ -\dfrac{\partial \mathcal{E}}{\partial q} - gh\sigma_2 \dfrac{\partial S_f}{\partial q} \end{pmatrix}. \end{aligned} \tag{18}$$

Equations (15) and (17) can be solved using the same numerical technique. In this case, both are solved using a finite volume formulation using an explicit Euler scheme for the time integration and a FOU scheme for the spatial integration (Burguete & García-Navarro 2004). For a given cell i with edges $i - 1/2$ and $i + 1/2$, a locally linearized problem is formulated. Using an upwind Riemann solver, the updating expression for the physical equations follows the scheme:

$$\mathbf{U}_i^{n+1} = \mathbf{U}_i^n - \frac{\Delta t}{\Delta x}\left(\sum_{p=1}^{2} (\tilde{\lambda}^+ \gamma \tilde{\mathbf{e}})_{i-1/2}^p + \sum_{p=1}^{2} (\tilde{\lambda}^- \gamma \tilde{\mathbf{e}})_{i+1/2}^p\right)^n, \tag{19}$$

where Δt is the integration time step and Δx the distance between the center of each computational cell. The updating procedure (19) takes into account the sign of the contribution $\tilde{\lambda}^{\pm} = 0.5(\tilde{\lambda} \pm |\tilde{\lambda}|)$ from each edge, where the approximate eigenvalues can be defined

as $\tilde{\lambda}^1 = \tilde{u} - \tilde{c}$, $\tilde{\lambda}^2 = \tilde{u} + \tilde{c}$ and the eigenvectors are $\tilde{\mathbf{e}}_\mathbf{2}^T = (1, \tilde{\lambda}^2)$, $\tilde{\mathbf{e}}_\mathbf{2}^T = (1, \tilde{\lambda}^2)$. This compact formulation requires one to define $\tilde{\gamma}^p = (\tilde{\alpha} - \tilde{\beta}/\tilde{\lambda})^p$ with:

$$\tilde{\alpha}^1 = \frac{1}{2\tilde{c}}((\tilde{u} + \tilde{c})\delta h - \delta q), \quad \tilde{\alpha}^2 = \frac{1}{2\tilde{c}}((\tilde{u} - \tilde{c})\delta h + \delta q), \tag{20}$$

and

$$\tilde{\beta}^1 = \frac{1}{2c}g\tilde{h}(\delta z - \Delta x\tilde{S}_f), \tag{21}$$

where the source term contribution $\tilde{\beta}$ satisfies $\tilde{\beta}^2 = -\tilde{\beta}^1$. It is also worth mentioning that the linearized source terms β^p are discretized using an upwind scheme.

The terms denoted $\delta(\cdot)$ refer to differences between the right and left states of each cell $\delta(\cdot) = ()_r - ()_l$, while $\tilde{(\cdot)}$ are averaged values $\tilde{(\cdot)} = 0.5[(\cdot)_r + (\cdot)_l]$. It is important to note that this notation is valid only in the numerical scheme framework and it is different from the one used in the adjoint system deduction where $\delta(\cdot)$ denoted the variation operator in time–space domain.

On the other hand, the lateral discharge can be considered centered in the cell as a variation of water depth:

$$h^{n+1} = h^{n+1/2} + \frac{q_l^n \Delta t}{\Delta x} \tag{22}$$

integrated in the time step as an update after contributions are computed ($h^{n+1/2}$) considering the previous water depth for the estimation of the outlet discharge q_l^n.

The same discretization can be applied to the adjoint system (17), leading to the expression:

$$\mathbf{\Psi}_i^n = \mathbf{\Psi}_i^{n+1} + \frac{\Delta t}{\Delta x}\left(\sum_{p=1}^{2}(\tilde{\lambda}_\Psi^+\gamma_\Psi\tilde{\mathbf{e}}_\mathbf{\Psi})_{i-1/2}^p + \sum_{p=1}^{2}(\tilde{\lambda}_\Psi^-\gamma_\Psi\tilde{\mathbf{e}}_\mathbf{\Psi})_{i+1/2}^p\right)^{n+1} \tag{23}$$

where several differences from (19) can be observed. First, the time integration must be performed by a forward Euler scheme, marching back in time. It is important to appreciate the superscript related to the dependence on the previous time step. On the other hand, the approximate eigenvalues for (23) satisfy $\tilde{\lambda}_\Psi^1 = -\tilde{\lambda}^2$ and $\tilde{\lambda}_\Psi^2 = -\tilde{\lambda}^1$ implying that $\tilde{\mathbf{e}}_{\mathbf{\Psi 1}}^T = (\tilde{\lambda}_\Psi^2, 1) = (-\tilde{\lambda}^1, 1)$, $\tilde{\mathbf{e}}_{\mathbf{\Psi 2}}^T = (\tilde{\lambda}_\Psi^1, 1) = (-\tilde{\lambda}^2, 1)$ and $\tilde{\gamma}_\Psi^p = (\tilde{\alpha}_\Psi - \tilde{\beta}_\Psi/\tilde{\lambda}_\Psi)^p$ with:

$$\begin{aligned}
&\tilde{\alpha}_\Psi^1 = \frac{1}{2\tilde{c}}((\tilde{u} + \tilde{c})\delta\sigma_2 + \delta\sigma_1), \quad \tilde{\alpha}_\Psi^2 = \frac{1}{2\tilde{c}}((-\tilde{u} + \tilde{c})\delta\sigma_2 - \delta\sigma_1)\\
&\tilde{\beta}_\Psi^1 = \frac{1}{2\tilde{c}}((\tilde{u} + \tilde{c})\tilde{R}_2 + \tilde{R}_1), \qquad \tilde{\beta}_\Psi^2 = \frac{1}{2\tilde{c}}((-\tilde{u} + \tilde{c})\tilde{R}_2 - \tilde{R}_1)
\end{aligned} \tag{24}$$

with

$$\begin{aligned}
\tilde{R}_1 &= \Delta x(g\tilde{\sigma}_2[\tilde{S}_0 - \tilde{S}_f - \tilde{h}\partial_h\tilde{S}_f] + \sigma_1\partial_h\tilde{q}_l)\\
\tilde{R}_2 &= \Delta x(-g\tilde{h}\tilde{\sigma}_2\partial_q\tilde{S}_f).
\end{aligned} \tag{25}$$

Additionally, contributions regarding $(\partial_h\mathcal{E})$ are integrated in the cell i where measurement takes place. One may write:

$$\partial_h\mathcal{E}_i = \begin{pmatrix} 2(h_i - h_{obj,i}) & \text{if } x_i = x_{im} \\ 0 & \text{otherwise.} \end{pmatrix} \tag{26}$$

As information from the SWE is required for the adjoint equation, first the forward-in-time SWE and then the backward-in-time adjoint system can be solved leading to the final value problem. Due to the similarities in their eigenvalues, they can be solved using the same time step size. The explicit Euler integration requires a suitable Δt bounded by the Courant–Friedrichs–Lewy (CFL) condition to ensure the numerical stability (LeVeque 2002). For the numerical scheme presented, this restriction requires that in cell i the wave celerity λ^p satisfies:

$$\Delta t = \text{CFL}\min_{i,p}\left(\frac{\Delta x}{|\tilde{\lambda}^p|_{i+1/2}}\right), \qquad \text{CFL} \leq 1. \tag{27}$$

One of the most representative drawbacks when solving the adjoint PDEs is the requirement to store information about the physical system at all points in time. The impact in terms of memory requirements can be estimated as $\mathcal{O}(n^2)$ taking into account that, in the one-dimensional case, not only the number of cells, but also the required time steps to perform the computation are not too large.

Typically when using the 1D approach, problems that model tenths of kilometers using hundreds of cells require minutes to simulate days.

MATHEMATICAL OPTIMIZATION

Mathematical optimization can be understood as the process of searching for the optimal value that minimizes a given functional. This searching can be done using different techniques. They are usually classified into two main groups: gradient-based and gradient-free optimizers. The former option requires the evaluation of the gradient for use as a guide when looking for the optimum. This is very efficient when dealing with convex problems. Gradient-free methods perform the operation over the whole domain and they are very convenient when multi-modal and noisy functions need to be minimized. These methods offer a suitable technique to cover the domain where the variable to be calibrated can be found.

The most relevant detail when dealing with the MC method is the *brute-force*-based methodology which is based on finding the optimum. In contrast to the gradient-based methods, MC just reduces the window for finding the optimal solution. Another important difference from the gradient-based methodology is the non-deterministic character of MC calibrations.

MC method

Gradient-free methods usually deal with global optimization problems where the whole process is based on heuristic and stochastic algorithms (Moles *et al.* 2003; Zabinsky 2013; Sedaghatdoost & Ebrahimian 2015). These methods include adaptive stochastic methods such as MC inspired methods. They look for the solution by random sampling. Instead of locating the optimal value by means of the information of the gradient, it is possible to cover the domain to seek the minimum and recursively reduce that domain. This reduction occurs when a set of the best options among all those evaluated is found. There is an interesting discussion of MC methods in Atanassov & Dimov (2008).

These stochastic methods are usually described as non-deterministic and the MC method is one of the most representative. The method is illustrated in Figure 2. Considering an initial interval $\mathcal{I}^0 \in (K^0_{g\,min}, K^0_{g\,max})$, N_{trials} random values of K_g are generated within this interval. Then, the functional (4) is evaluated for every single trial and the best of them defines the new sub-interval $\mathcal{I}^1 \subset \mathcal{I}^0$. This process is iterated until the maximum number of iterations is reached or until the functional fails to reach the target value. Further details can be found in Algorithm 1.

Result: A new value for K_g closer to the solution that minimizes **J**

input: N_{iter}, N_{trials}, $\mathcal{I}^0$, $tol_{\mathbf{J}}$ **output:** $K^m_g \mathrm{m} = 0$;
while $m \leq N_{iter} \wedge \mathbf{J}^m > tol_{\mathbf{J}}$ **do**
/* **Generate** N_{trials} **random trials within the interval** $\mathcal{I}^m$ */
$K_{g*} \in rand\,(K_{g\,inf}, K_{g\,sup})|(K_{g\,inf}, K_{g\,sup} \in I^m)$;
/* **Best values** K^m_{g1}, K^m_{g2} **defines the new interval** */
$\mathcal{I}^{m+1} \leftarrow (K^m_{g1}, K^m_{g2})|(\mathbf{J}_{K^m_1}, \mathbf{J}_{K^m_2} \leq \mathbf{J}_{K^m_i} \forall K^m_i \in \mathcal{I}^m)$;
$\mathbf{J}^m \leftarrow min(\mathbf{J}_{K^m_1}, \mathbf{J}_{K^m_2})$;
$K^m_g \leftarrow \arg\min_{K_g} \mathbf{J}^m$;
$m++$;

Algorithm 1: MC method.

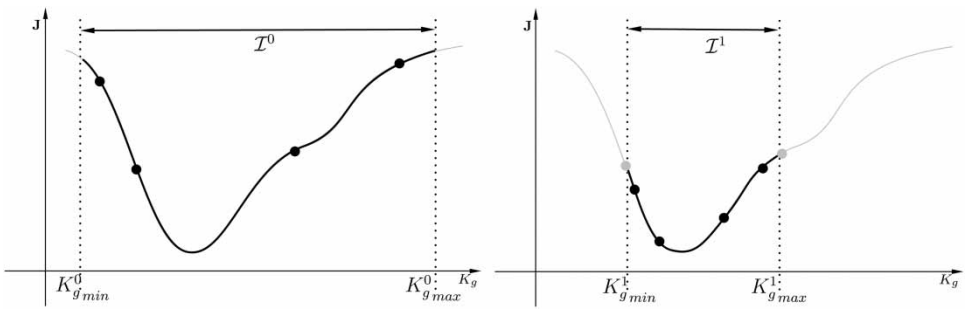

Figure 2 | Scheme of the MC-based optimization method. First iteration for a given interval I^0 (left) and following iteration with the sub-interval I^1 (right).

The whole computational cost of this method includes the evaluation of each trial. If the method has not converged before $tol_{\mathbf{J}}$ or N_{iter} is reached, the computational cost is $C_{MC} = N_{iter} \times N_{trials}$ in terms of the number of simulations. While the method does not require additional parameters, the complexity comes from the definition of the number of seeds that the method has to include at each time. The trade-off between the maximum number of iterations, N_{iter}, and the number of elements generated per iteration, N_{trials}, is not easy to balance.

Gradient-descent method

For gradient-based optimization, information about the sensitivity of the performance function with respect to the calibrated variable (K_g) is required. In other words, the error and the parameter to be controlled need to be related in some way. Using (11c), and recalling that perturbations are not introduced for (h, q), the relation between the error and the parameter K_g to be controlled can be expressed as follows:

$$\delta\mathbf{J} = \int_{x_0}^{x_L}\int_0^T \sigma_1 \frac{\partial q_l}{\partial K_g}\delta K_g dt dx. \tag{28}$$

Then, $\nabla\mathbf{J}$ can be calculated as:

$$\nabla\mathbf{J} = \frac{\delta\mathbf{J}}{\delta K_g}\bigg|_{x=x_c} = \int_0^T \left[\sigma_1 \frac{\partial q_l}{\partial K_g}\right]\bigg|_{x=x_c} dt, \tag{29}$$

considering x_c as the position of the lateral gate. Using (29) it is possible to perform the calibration with a gradient-based optimizer. The simplest is the implementation of the GD method (Nocedal & Wright 2006) following the $p^m = \nabla\mathbf{J}^m$ direction by means of:

$$K_g^{m+1} = K_g^m - \epsilon^m p^m \tag{30}$$

where m denotes the iteration of the method and ϵ^m denotes the step-length used by the method. The optimization procedure using this method is illustrated in Figure 3. Considering the initial value of K_g^0 and obtaining the value of $\nabla\mathbf{J}^0$, descent is performed with step-size ϵ^0, leading to the new value of K_g^1.

The integration of (30) in the full optimization procedure is detailed in Algorithm 2.

Result: A new value for K_g closer to the solution that minimizes $\mathbf{J}$ **input:** K_g^0, ϵ^0, $tol_{\mathbf{J}}$, $tol_{\nabla\mathbf{J},max}$, $tol_{\delta K_g,max}$, N_{iter} **output:** K_g^m

```
m = 0;
while m ≤ N_iter ∧ J(K_g^m) > tol_J do
  K_g^{m+1} ← K_g^m − ε^m ∇J^m;
  if ||∇J(K_g^{m+1})|| ≤ tol_{∇J,max} then
    /* converged on critical point                    */
    return;
  else
    if ||K_g^{m+1} − K_g^m|| ≤ tol_{δK_g,max} then
    /* converged on an K_g value                      */
    return;
    else
      if J(K_g^m) < J(K_g^{m+1}) then
      /* It has diverged                              */
    ε^{m+1} = 0.5ε^m;
    else
    ε^{m+1} = 1.1ε^m;
    m++;
```

Algorithm 2: Gradient-descent method.

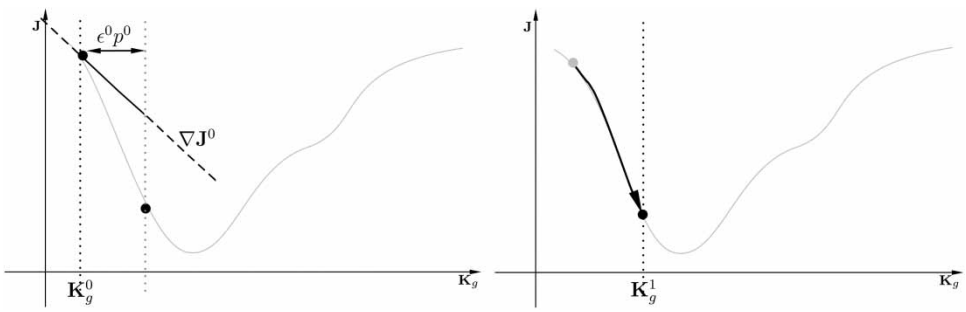

Figure 3 | Scheme of the gradient-descent method. Evolution of K_g from K_g^0 (left) to K_g^1 (right) following the direction $\nabla\mathbf{J}^0$.

The algorithm includes a little modification from the classical gradient-descent method regarding the step-length used in the optimization. When using the fixed step-length $\epsilon^m = \epsilon$, convergence is not guaranteed. This is because there are situations in which, when *overshooting* a long way using some value of the gradient, the method may diverge. A typical strategy is the use of an initial ϵ that may be increased by a constant factor (1.1 for example) or halved if the functional estimation is amplified. Nonetheless, more sophisticated step-sizes can be applied (Yuan 2008).

The cost of this optimizer considering the computation of the gradient using the adjoint variables is $C_{GD} = (c_{sw} + c_{adj}) \times N_{iter}$ where c_{sw} is the computational cost of the forward shallow water model run and c_{adj} is the cost of the adjoint solver. The amount of computational effort C_{GD} can be approximated by $C_{GD} \approx 2 \times c_{sw} \times N_{iter}$ since each iteration needs to solve the problem forwards and backwards in time, and they require the same number of integration time steps as well as the same number of computational operations. Comparing both, the cost of the stochastic method C_{MC} and the cost of the gradient-based method C_{GD}, the performance in terms of evaluations varies depending on: (1) the convergence ratio: whether MC employs the best trials or the gradient method uses faster directions will determine the number of iterations required to find the optimum; and (2) the initial guess/initial interval: the distance of the initial guess to the optimal solution as well as the definition of the adequate interval may have an important impact on the performance of the method.

Additionally, and for each method, the correct choice of the step-size in the gradient-descent method, or the number of trials used in each iteration in the case of stochastic optimization, may also degrade or improve the performance of the method.

The gradient-based method shows an intrinsic weakness compared with the MC method. While each trial of the MC method can be performed in parallel (each simulation can be computed independently), the parallelization of the gradient-based method requires the parallelization of the numerical solver, which is more complicated. In this work, both methods have been analyzed in sequential mode, which means that each trial is run after the previous trial has finished as in the case of the gradient method.

TEST CASES

In order to benchmark the previously introduced optimization methods, the gradient-based optimization method based on adjoint equations is compared with a MC optimization method. Due to its stochastic nature, MC results can change between one repetition and the next. Nevertheless, this effect has not been analyzed in this work. In addition, the computational cost of both methods is defined as the number of simulations required to converge to the desired state. Otherwise, the measurements may be misleading, because MC processes are intrinsically independent; thus, they may be directly parallelized. In the case of the gradient-based method, the computational optimization of the technique must be applied to the solver of both the direct and the adjoint models. Due to this, performance of each method is evaluated in terms of the number of simulations required to reach their objective functions.

The benchmark canal with length $L = 1{,}000\ m$ is defined by a constant rectangular unitary width section with $x \in [-500, 500]$. The channel is defined with a constant Gauckler–Manning's roughness coefficient of $n = 0.01\ s/m^{1/3}$ and a constant slope of 0.011 (see Figure 4).

The optimizers are configured using the same tolerance $tol_{\mathbf{J}} = 10^{-5}$ and, in the case of GD, that tolerance is also used for $tol_{\delta K_g}$ and $tol_{\nabla \mathbf{J}}$. The initial interval for MC covers the entire search domain for the coefficient K_g that is $\mathcal{I}^0 = (0, \sqrt{2g})$. Furthermore, it is configured to perform the calibration with $N_{iter} = N_{trials} = 8$.

The step-size range for the gradient method is $\epsilon \in (0.0001, 50.0)$ and the initial step-size is defined differently in each case.

Test case I

In the first test case, one lateral gate is located at $x_{g1} = 300\ m$ and the measured or desired water depth is defined at $x_m = 250\ m$ (see Figure 4). The target function h_{obj} is also plotted in Figure 4.

A constant inlet of $q = 2.2627\ m^2/s$ is assumed to define the initial steady state condition for the simulated case and is kept constant at all times. Regarding these conditions and using (3), it is possible to find some K_g to adjust the

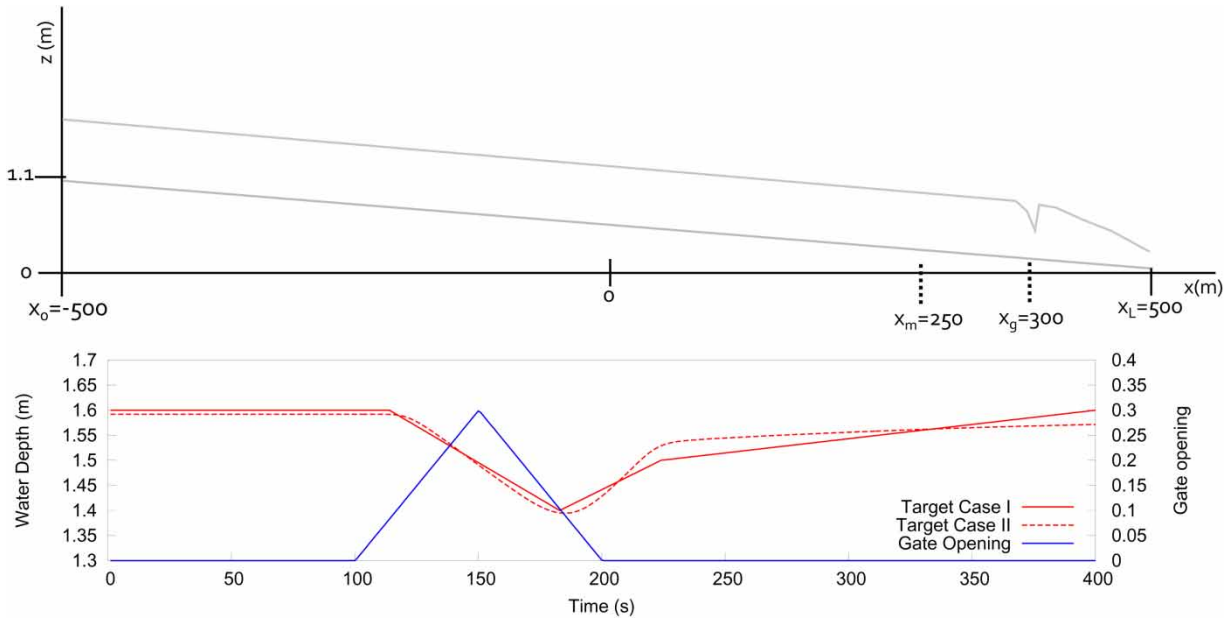

Figure 4 | Sketch of the configuration used in Test case I and II, with the location x_m of the probe and the location x_g of the lateral gate (upper panel). The lower panel includes objective water depth h_{obj} at $x_m = 250m$ for Test case I and for Test case II and y_2 axis represents gate opening (m).

results to the objective water depth h_{obj}. This h_{obj} is an *invented* analytic function which does not correspond to any realistic water depth measurement and is used only for demonstrating that this method is able to adjust the parameter even when the measurement does not correspond to any possible solution. The GD method is configured with $\epsilon^0 = 1.0$. Additionally, the initial guess for the method is $K_g^0 = 1.35$.

With this configuration, the gradient method required ten steps to complete the optimization process, reaching $\mathbf{J} = 3.09335 \cdot 10^{-1}$ and $\mathbf{J} = 3.09335 \cdot 10^{-1}$ when using the MC method (see Figures 5 and 6). The last iteration finds the best $K_g = 2.46214$ in the interval of $K_g \in (2.45090, 2.50456)$. The functional is reduced until $\mathbf{J} = 3.10645 \cdot 10^{-1}$. While the MC method does not reach the stop-criteria, the GD method converges to a critical point due to $\nabla\mathbf{J} \leq tol_{\nabla\mathbf{J}}$.

Figure 7 displays the variation of the functional with the empirical value K_g. Note that the variation is smooth. In this case, the MC method rapidly locates the region of the optimum.

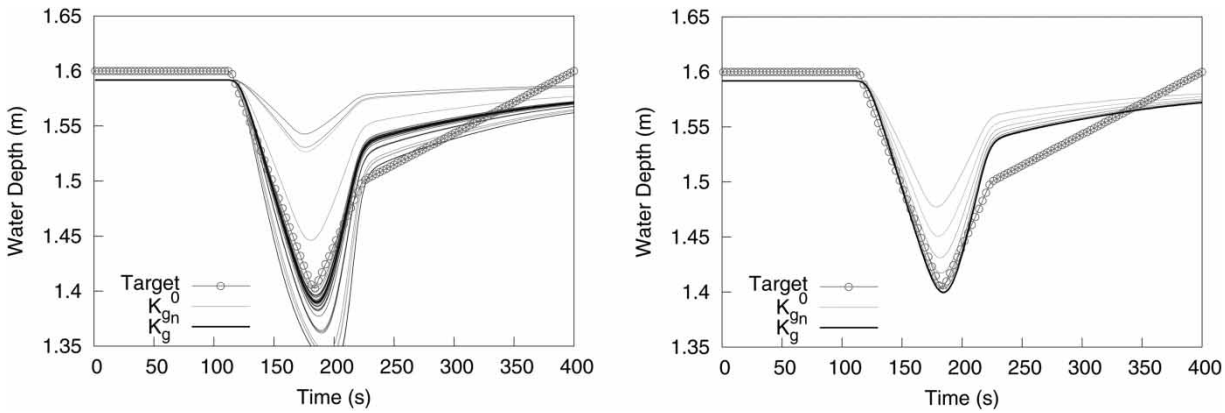

Figure 5 | Test case I: Evolution of the water depth at $x_m = 250m$ through the calibration process for MC (left) and GD (right) methods.

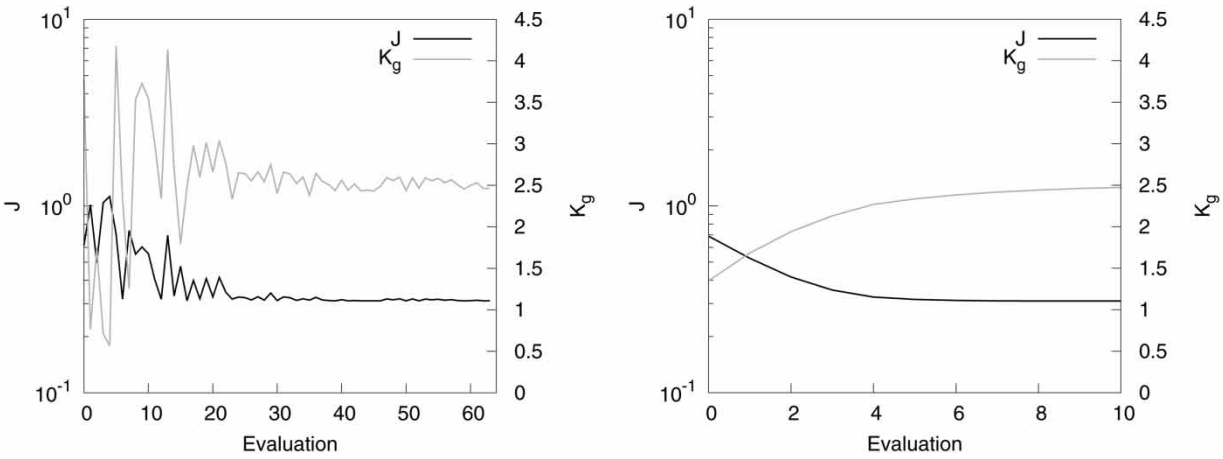

Figure 6 | Convergence of the error and K_g for Test case I using MC (left) and GD (right).

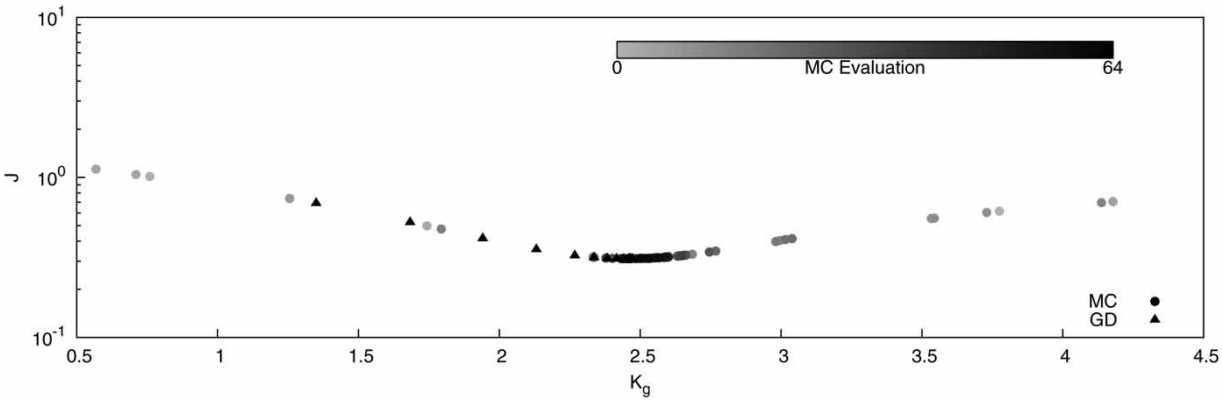

Figure 7 | Test case I: Evolution of **J** with respect to K_g for each method. Dots represent the different MC evaluations.

Test case II

For the second test case, the objective water depth history is defined by the depths recorded during a previous simulation run with $K_g = 2.46027$. The setup is essentially the same as the previous one, replacing designed conditions with simulated results. Theoretically, the minimum of the functional in this case should be min $\mathbf{J} = 0$. As the gradient method may require some stop condition as a convergence criterion, the tolerance is established to $tol_J = 10^{-4}$. Moreover, the initial K_g for the gradient method is defined further than in the previous case $K_g^0 = 0.1$.

Using this configuration, the GD method only requires seven steps to converge to $K_g = 2.46065$ with $\mathbf{J} = 2.31662 \cdot 10^{-4}$, while using the MC method the optimizer provides $K_g = 2.46214$ and is unable to converge to a better result, obtaining $\mathbf{J} = 9.79302 \cdot 10^{-4}$ (see Figures 8 and 9).

As in the previous case, the GD method shows a higher convergence rate. Not only the speed that the GD method reaches when obtaining the solution, but also the quality of the method providing the gradient estimation is highlighted. While requiring the equivalent of two simulations for each gradient step, the convergence ratio for each iteration is higher than for the MC method. Moreover, GD strictly converges to an optimal value of K_g since $tol_{\delta f,max}$ is reached. In contrast, the MC method reaches its maximum number of iterations without reaching the tolerance.

In Figure 10, the functional **J** is plotted against the different values of K_g obtained by each method. It is possible to

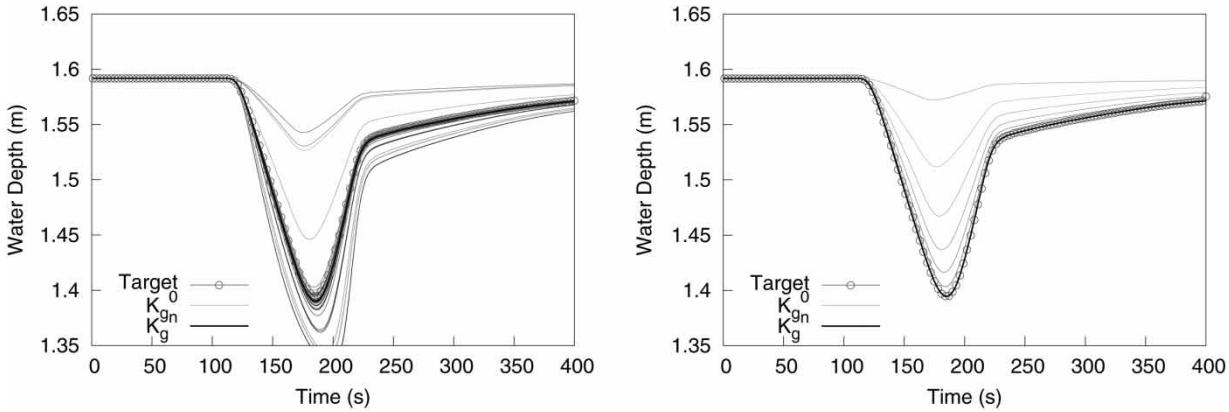

Figure 8 | Test case II: Evolution of the water depth at $x_m = 250m$ through the calibration process for MC (left) and GD (right) methods.

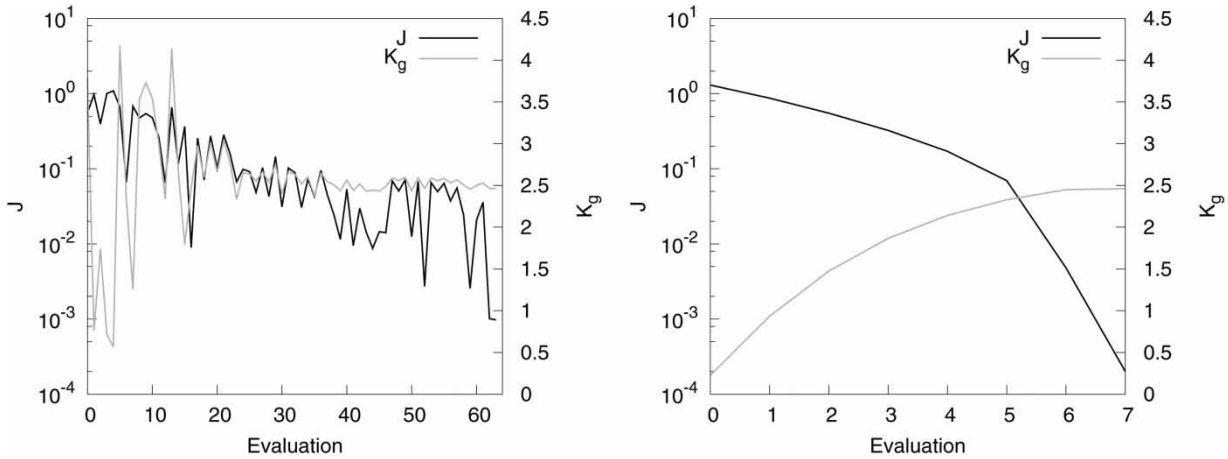

Figure 9 | Convergence of the error and K_g for Test case II using MC (left) and GD (right).

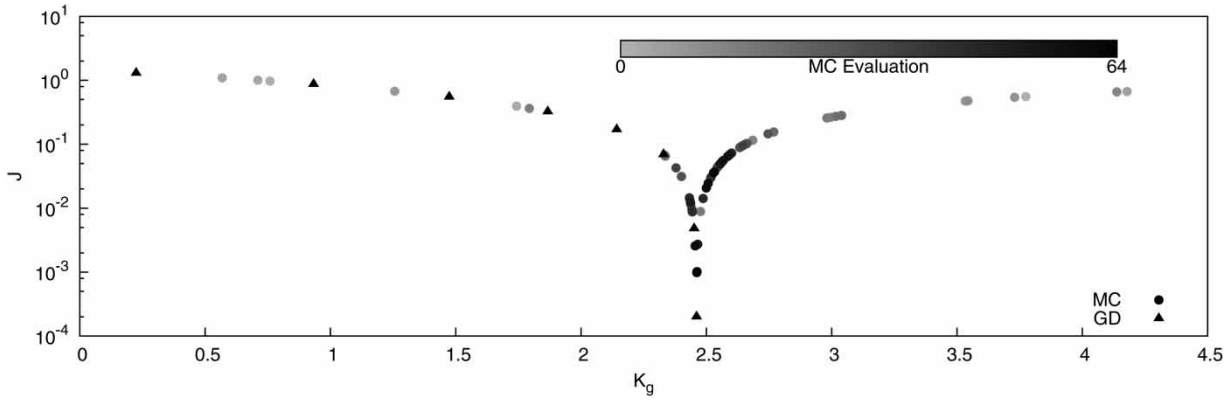

Figure 10 | Test case II: Evolution of **J** with respect to K_g for each method. Dots represent the different MC evaluations.

observe how the GD method describes the curve better and faster than the MC method.

Test case III

The third test case is a variation of the second. In this case, two transverse gates have been included. There are several techniques for dealing with such structures in the model. For instance, in Cozzolino *et al.* (2015), a robust and efficient numerical treatment is incorporated into the numerical method, providing a dynamic detection of free and submerged regimes. In the present work, they have been formulated as internal boundary conditions following Morales-Hernández *et al.* (2013), which provides a simpler method good enough for relatively uniform flow regimes. The idea is to analyze the possible influence that these internal boundaries have over the control.

The main channel is the same as in the previous cases. Additionally, two cross gates have been included at $x_1 = -333\,m$ and $x_2 = 333\,m$. The lateral gate is between these gates, located at $x_g = 0\,m$. A sketch of the channel is shown in Figure 11.

A forward simulation using $K_g = 1.35$ was performed previously and the temporal evolution at $x_m = 300\,m$ is used as the target water depth.

This configuration includes the influence of the internal boundaries on the calibration process. The result of the calibration process for both the MC method and the GD method is displayed in Figure 12.

The result of the calibration using the stochastic methodology provides bounds on the optimal solution $K_g \in (1.2621, 1.2837)$ with the best option within the interval of $K_g = 1.2639$ with an error of $\mathbf{J} = 2.49562 \cdot 10^{-2}$. The GD calibration calculates $K_g = 1.35018$ with $\mathbf{J} = 1.067 \cdot 10^{-4}$. The number of steps for non-gradient optimizations required in the process includes 64 forward simulations, while in the case of the gradient-based simulation only seven are required, and seven more for the adjoint system integration. It represents an acceleration of $s_{up} = 64/(7+7) = 4.57$ of the GD method against the MC method.

This case has detected one of the most relevant weaknesses of the MC method: it may not converge to the optimal solution. As in the previous case, the GD method converges to an optimal value of K_g.

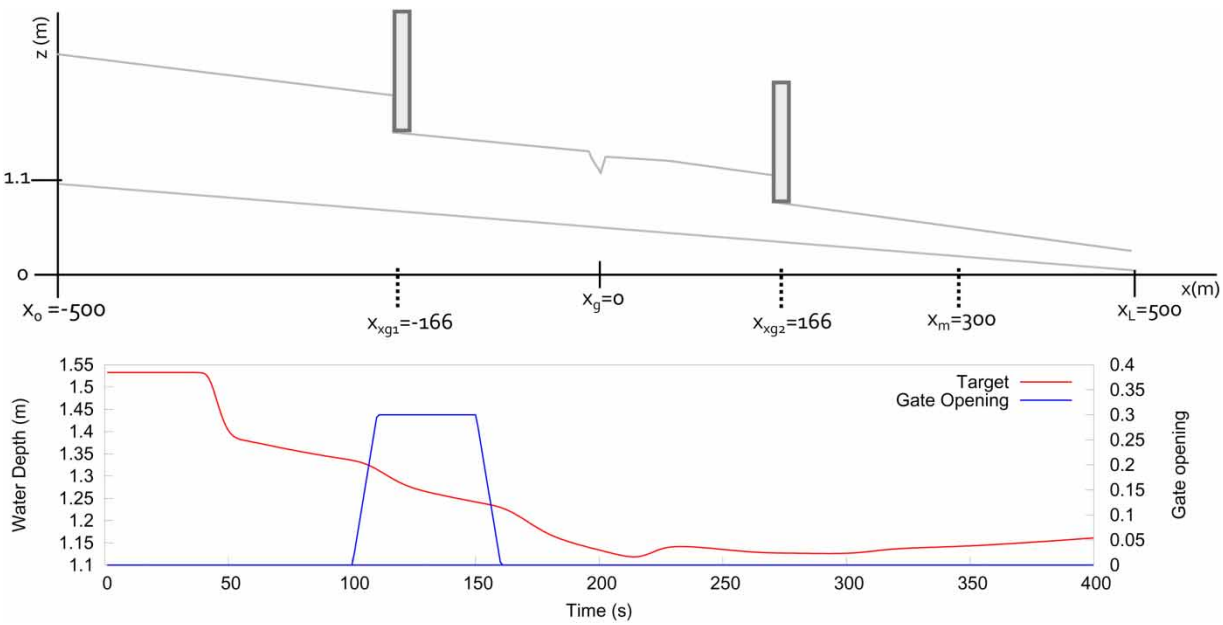

Figure 11 | Sketch of the channel and the location of the probe (x_m), the lateral gate (x_g), and the two cross gates (x_{xg1}, x_{xg2}). The lower panel includes objective water depth h_{obj} at $x_m = 300\,m$ for Test case III and y_2 axis represents gate opening (m).

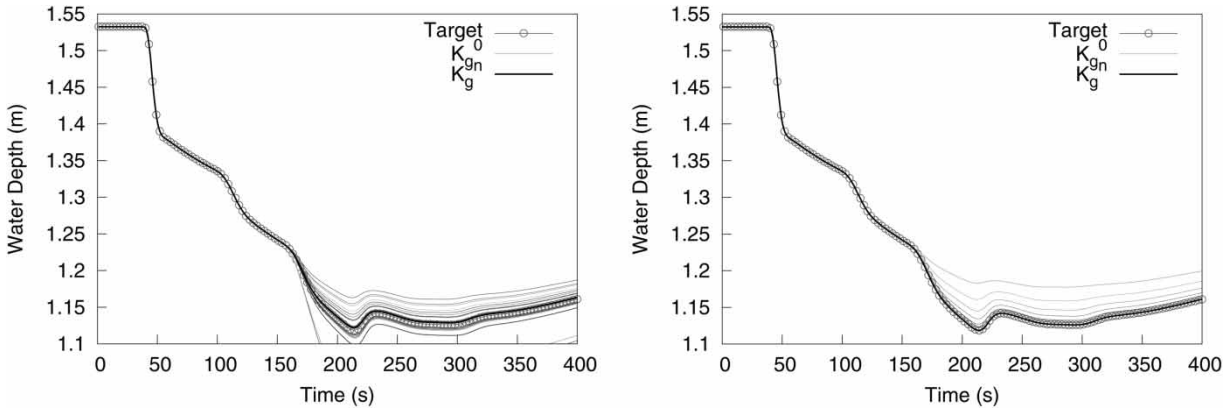

Figure 12 | Test case III: Evolution of the water depth at $x_m = 250$ through the calibration process for MC (left) and GD (right) methods.

The GD method has been configured using the step-length of $\epsilon_0 = 5.0$. It is notable that, if using $\epsilon_0 = 1.0$ as in Test cases I and II, the number of steps required grows to 16. On the contrary, the MC model does not converge to an optimum solution (K_g), not even using the predefined eight maximum iterations. In this case, and in one step, it is found that the optimum probably lies within the interval (1.2620925, 1.283715). In Figure 13, this fact can be particularly appreciated. Note that this behavior is the opposite of that observed in the previous experiment and displayed in Figure 10.

As this location has been found, it is not possible to go on from there and improve the solution, even by increasing the number of steps in the method, because each step will be a subset of the previous one. Considering the definition of the functional at iteration $n+1$ of the MC method $\mathbf{J}^{n+1}$ as:

$$\mathbf{J}^{n+1} = \min\left(\mathbf{J}(K_1^{n+1}), \mathbf{J}(K_2^{n+1}), \ldots, \mathbf{J}(K_{N_{trials}}^{n+1})\right), \tag{31}$$

the following property is satisfied:

$$\mathbf{J}^{n+1} \leq \max \mathbf{J}(K_\alpha),\ K_\alpha \in \mathcal{I}^n. \tag{32}$$

When an interval that does not contain the minimum is found, the method is not strictly convergent in the sense of $\mathbf{J}^{n+1} < \mathbf{J}^n$ but property (32) is always satisfied as can be observed in the results of Figure 14. Nevertheless, this could be improved by increasing the number of MC processes used in each iteration, which implies more

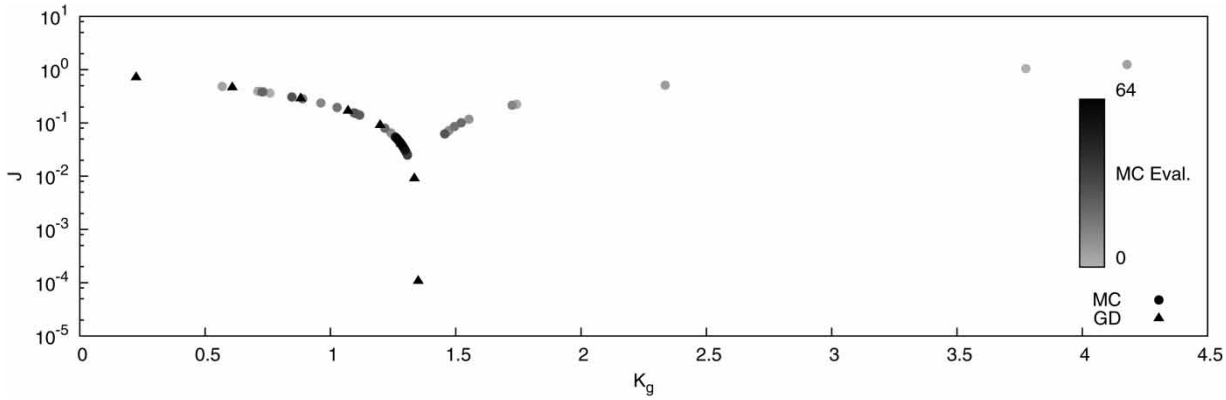

Figure 13 | Test case III: Evolution of **J** with respect to K_g for each method. Dots represent the different MC evaluations.

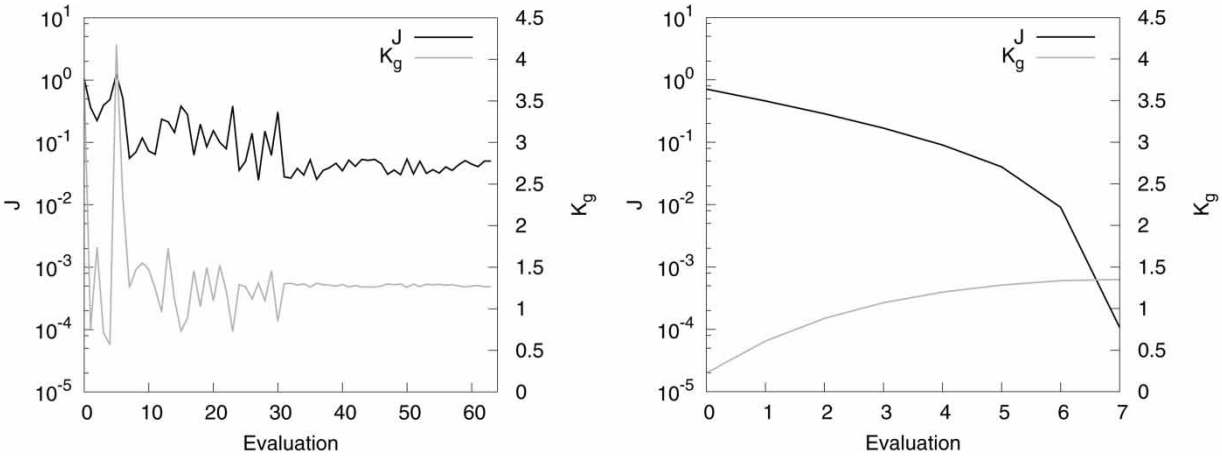

Figure 14 | Convergence of the error and K_g for Test case III using MC (left) and GD (right).

resolution in the searching lattice. In Dotto *et al.* (2012), a deep analysis of the application of the MC method highlights the dependence of the convergence ratio on the number of trials analyzed and the threshold used. This also implies an increase in the number of simulations. Not only the quality of the calibration in terms of convergence rate, but also the quantity of steps in the process, establish strong differences between these methodologies.

These results highlight a new possibility, where a combination of these methods can obtain the solution more quickly. The MC method can be used to generate the initial guess for the GD method, which then can be used to descend more rapidly to the optimal solution.

CONCLUSIONS

In this work the comparison of a MC-based optimization and an adjoint method-based optimization method to calibrate discharge coefficients of lateral gates on 1D channels is presented. The techniques have been checked using three test cases.

The adjoint technique has the drawback of the non-generalized way of calculating sensitivities. However, when developing it for a particular PDE system, it offers a powerful procedure for performing optimal control. Being a gradient-based method, it requires the evaluation of the error gradient. The present work has been based on a simple semi-fixed, step-length algorithm which, in some cases, may vary the performance depending on the step-length used. Other gradient-based methods such as BFGS or L-BFGS may be used with the previous information, including an optimal step-length that may improve the convergence rate of the method.

On the contrary, MC methods are capable of obtaining good results with a simpler implementation for this type of problem. Previous information, other than the range where the optimal solution may be found, is not required. This is an advantage when calibration is related to an ill-posed problem or a complex functional, but not for such cases as those presented in this work.

The MC method provides two advantages: independence from the model to be calibrated and the intrinsic capability of working in parallel. On the other hand, the GD method shows a greater convergence rate, but it is sensitive to the initial guess used. Results suggest that a combination of these methods, the MC method for choosing the initial guess and then the GD method for descending in the correct direction, may generate an effective optimization method. The main disadvantage of the GD method based on the adjoint formulation is that it must be carefully reformulated in each different application.

Future work may include the advantage of MC in choosing an appropriate initial guess for use in the gradient-based optimizer. Moreover, the same technique may be applied to the 2D system of equations. However, limitations on the time–space dimension of the problem may be found due to the memory storage requirements of the adjoint method.

Nevertheless, more sophisticated objective functions and optimization applications can be addressed in the two-dimensional framework, where calibration is a very common task in practical applications. It is also feasible to develop a very similar technique for related uses, such as the calibration of the friction coefficient used in Manning's formula following the steps presented in the first part of the work and then comparing both methods for this application.

ACKNOWLEDGEMENTS

This research was partially funded by the Spanish MINECO/FEDER through the Research Project CGL2015-66114-R and by Diputación General de Aragón, DGA, through FEDER funds. The first author was also supported by the Spanish Ministry of Economy and Competitiveness fellowship BES-2012-053691.

REFERENCES

Atanassov, E. & Dimov, I. T. 2008 What Monte Carlo models can do and cannot do efficiently? *Appl. Math. Model.* **32** (8), 1477–1500.

Baume, J.-P., Malaterre, P.-O., Belaud, G. & Le Guennec, B. 2005 Sic: a 1D hydrodynamic model for river and irrigation canal modeling and regulation. *Métodos Numéricos em Recursos Hídricos* **7**, 1–81.

Bueno-Orovio, A., Castro, C., Palacios, F. & Zuazua, E. 2012 Continuous adjoint approach for the Spalart-Allmaras model in aerodynamic optimization. *AIAA J.* **50** (3), 631–646.

Burguete, J. & García-Navarro, P. 2004 Improving simple explicit methods for unsteady open channel and river flow. *Int. J. Numer. Meth. Fluids* **45** (2), 125–156.

Burguete, J. & Latorre, B. 2015 MPCOTool: the multi-purposes calibration and optimization tool. Available at: https://github.com/jburguete/mpcotool.

Burguete, J., Lacasta, A. & García-Navarro, P. 2014 SURCOS: A software tool to simulate irrigation and fertigation in isolated furrows and furrow networks. *Comput. Electron. Agr.* **103**, 91–103.

Cassel, K. W. 2013 *Variational Methods with Applications in Science and Engineering.* Cambridge University Press, Cambridge.

Castro, C., Lozano, C., Palacios, F. & Zuazua, E. 2007 Systematic continuous adjoint approach to viscous aerodynamic design on unstructured grids. *AIAA J.* **45** (9), 2125–2139.

Chanson, H. 2004 *Hydraulics of Open Channel Flow.* Butterworth-Heinemann, Oxford, UK.

Chaparro, B., Thuillier, S., Menezes, L., Manach, P. & Fernandes, J. 2008 Material parameters identification: gradient-based, genetic and hybrid optimization algorithms. *Comp. Mat. Sci.* **44** (2), 339–346.

Chaudhry, M. H. 2007 *Open-Channel Flow.* Springer Science & Business Media, Berlin.

Cozzolino, L., Cimorelli, L., Covelli, C., Della Morte, R. & Pianese, D. 2015 The analytic solution of the shallow-water equations with partially open sluice-gates: the dam-break problem. *Adv. Water Resour.* **80**, 90–102.

Cunge, J. A., Holly, F. M. & Verwey, A. 1980 *Practical Aspects of Computational River Hydraulics.* Pitman Advanced Publishing Program, Boston, MA.

Díaz, M. C., López-García, J. & Parés, C. 2013 High order exactly well-balanced numerical methods for shallow water systems. *J. Comput. Phys.* **246**, 242–264.

Ding, Y. & Wang, S. S. 2005 Identification of Manning's roughness coefficients in channel network using adjoint analysis. *Int. J. Comput. Fluid. Dyn.* **19** (1), 3–13.

Ding, Y. & Wang, S. S. 2006 Optimal control of open-channel flow using adjoint sensitivity analysis. *J. Hydraul. Eng.-ASCE* **132** (11), 1215–1228.

Dotto, C. B., Mannina, G., Kleidorfer, M., Vezzaro, L., Henrichs, M., McCarthy, D. T., Freni, G., Rauch, W. & Deletic, A. 2012 Comparison of different uncertainty techniques in urban stormwater quantity and quality modelling. *Water Res.* **46** (8), 2545–2558.

Fovet, O., Litrico, X. & Belaud, G. 2010 Modeling and control of algae detachment in regulated canal networks. In *Control Applications (CCA), 2010 IEEE International Conference on*, IEEE, pp. 1881–1886.

Fread, D. L. & Smith, G. F. 1978 Calibration technique for 1-d unsteady flow models. *J. Hydraul. Div. -ASCE* **104** (7), 1027–1044.

Giles, M. & Glasserman, P. 2006 Smoking adjoints: fast Monte Carlo Greeks. *Risk* **19** (1), 88–92.

Giles, M. B. & Pierce, N. A. 2000 An introduction to the adjoint approach to design. *Flow, Turbul. Combust.* **65** (3–4), 393–415.

Henderson, F. M. 1966 *Open Channel Flow. Macmillan Series in Civil Engineering.* Macmillan, New York.

Hou, J., Liang, Q., Zhang, H. & Hinkelmann, R. 2015 An efficient unstructured MUSCL scheme for solving the 2D shallow water equations. *Environ. Modell. Softw.* **66**, 131–152.

Kesserwani, G. & Liang, Q. 2015 RKDG2 shallow-water solver on non-uniform grids with local time steps: application to 1D and 2D hydrodynamics. *Appl. Math. Model.* **39** (3), 1317–1340.

Kesserwani, G., Caviedes-Voullième, D., Gerhard, N. & Müller, S. 2015 Multi wavelet discontinuous Galerkin h-adaptive shallow water model. *Comput. Methods Appl. Mech. Eng.* **294**, 56–71.

Lacasta, A. & García-Navarro, P. 2016 A GPU accelerated adjoint-based optimizer for inverse modeling of the two-dimensional shallow water equations. *Comput. & Fluids* **136**, 371–383.

Lacasta, A., Caviedes-Voullième, D. & García-Navarro, P. 2015a Application of the adjoint method for the reconstruction of the boundary condition in unsteady shallow water flow simulation. In: *Proceedings of the 11th edition of the International Conference on Evolutionary and Deterministic Methods for Design, Optimization and Control with Applications to Industrial and Societal Problems*, pp. 1–16.

Lacasta, A., Morales-Hernández, M., Tejero-Juste, M., Burguete, J., Brufau, P. & García-Navarro, P. 2015b Validation and simulation of a regulated survey system through Monte Carlo techniques. *Ing. Agua* **19** (3), 117–133.

Lai, X. & Monnier, J. 2009 Assimilation of spatially distributed water levels into a shallow-water flood model. Part I: mathematical method and test case. *J. Hydrol.* **377** (1), 1–11.

LeVeque, R. J. 2002 *Finite Volume Methods for Hyperbolic Problems,* Vol. 31. Cambridge University Press, Cambridge.

Malaterre, P.-O., Rogers, D. C. & Schuurmans, J. 1998 Classification of canal control algorithms. *J. Irrig. Drain. E. -ASCE* **124** (1), 3–10.

Moles, C. G., Mendes, P. & Banga, J. R. 2003 Parameter estimation in biochemical pathways: a comparison of global optimization methods. *Genome Res.* **13** (11), 2467–2474.

Morales-Hernández, M., Murillo, J. & García-Navarro, P. 2013 The formulation of internal boundary conditions in unsteady 2-D shallow water flows: application to flood regulation. *Water Resour. Res.* **49** (1), 471–487.

Murillo, J. & García-Navarro, P. 2010 Weak solutions for partial differential equations with source terms: application to the shallow water equations. *J. Comput. Phys.* **229** (11), 4327–4368.

Murillo, J., García-Navarro, P. & Burguete, J. 2009 Time step restrictions for well-balanced shallow water solutions in non-zero velocity steady states. *Int. J. Numer. Meth. Fluids* **60** (12), 1351–1377.

Navas-Montilla, A. & Murillo, J. 2015 Energy balanced numerical schemes with very high order. The Augmented Roe Flux ADER scheme. Application to the shallow water equations. *J. Comput. Phys.* **290**, 188–218.

Nocedal, J. & Wright, S. 2006 *Numerical Optimization.* Springer Science & Business Media, New York.

Noelle, S., Pankratz, N., Puppo, G. & Natvig, J. R. 2006 Well-balanced finite volume schemes of arbitrary order of accuracy for shallow water flows. *J. Comput. Phys.* **213** (2), 474–499.

Pappenberger, F., Beven, K., Horritt, M. & Blazkova, S. 2005 Uncertainty in the calibration of effective roughness parameters in hec-ras using inundation and downstream level observations. *J. Hydrol.* **302** (1), 46–69.

Petaccia, G. & Savi, F. 2002 Numerical modelling of shock waves: simulation of a large number of laboratory experiments. In: *Proceedings of the International Conference in Fluvial Hydraulics, River Flow,* Vol. 1, pp. 449–458.

Piasecki, M. & Sanders, B. F. 2002 Optimization of multiple freshwater diversions in well-mixed estuaries. *J. Water Resour. Plan. Manage.* **128** (1), 74–84.

Sanders, B. F. & Katopodes, N. D. 2000 Adjoint sensitivity analysis for shallow water wave control. *J. Eng. Mech.-ASCE* **126** (9), 909–919.

Sedaghatdoost, A. & Ebrahimian, H. 2015 Calibration of infiltration, roughness and longitudinal dispersivity coefficients in furrow fertigation using inverse modelling with a genetic algorithm. *Biosystems Eng.* **136**, 129–139.

Wasantha Lal, A. 1995 Calibration of riverbed roughness. *J. Hydraul. Eng.-ASCE* **121** (9), 664–671.

Xing, Y., Zhang, X. & Shu, C.-W. 2010 Positivity-preserving high order well balanced discontinuous Galerkin methods for the shallow water equations. *Adv. Water Resour.* **33** (12), 1476–1493.

Xu, M., van Overloop, P. & van de Giesen, N. 2011 On the study of control effectiveness and computational efficiency of reduced Saint-Venant model in model predictive control of open channel flow. *Adv. Water Resour.* **34** (2), 282–290.

Yuan, Y. X. 2008 Step-sizes for the gradient method. *AMS IP Stud. Adv. Math.* **42** (2), 785.

Zabinsky, Z. B. 2013 *Stochastic Adaptive Search for Global Optimization,* Vol. 72. Springer Science & Business Media, New York.

First received 24 February 2016; accepted in revised form 28 October 2016. Available online 6 January 2017